Hydrogen Bonding to Tyrosyl Radical Analyzed by Ab Initio g-Tensor Calculations

ARTICLE *in* THE JOURNAL OF PHYSICAL CHEMISTRY A · MAY 2000

Impact Factor: 2.69 · DOI: 10.1021/jp0006633

Hydrogen Bonding to Tyrosyl Radical Analyzed by Ab Initio g-Tensor Calculations

Maria Engström,* Fahmi Himo,† Astrid Gräslund,‡ Boris Minaev,§ Olav Vahtras,|| and Hans Agren§

Department of Physics, Linköping University, SE-581 83 Linköping, Sweden

Received: February 18, 2000

Hydrogen bonding to the tyrosyl radical in ribonucleotide reductase (RNR) has been simulated by a complex between the phenoxyl radical and a water molecule. Multiconfigurational self-consistent field linear response theory was used to calculate the *g*-tensor of the isolated phenoxyl radical and of the phenoxyl−water model. The relevance of the model was motivated by the fact that spin density distributions and electron paramagnetic resonance (EPR) spectra of the phenoxyl and tyrosyl radicals are very similar. The calculated *g*-tensor anisotropy of the phenoxyl radical was comparable with experimental findings for tyrosyl in those RNRs where the H-bond is absent: $g_x = 2.0087(2.0087)$, $g_y = 2.0050(2.0042)$, and $g_z = 2.0025(2.0020)$, where the tyrosyl radical EPR data from *Escherichia coli* RNR are given in parentheses. The hydrogen bonding models reproduced a shift toward a lower g_x value that was observed experimentally for mouse and herpes simplex virus RNR where the H-bond was detected by electron−nuclear double resonance after deuterium exchange. This decrease could be traced to lower angular momentum and spin-orbit coupling matrix elements between the ground $^2B_1$ and the first excited $^2B_2$ states (oxygen lone-pair *n* to π_{SOMO} excitation) upon hydrogen bonding in a linear configuration. The g_x value was further decreased by hydrogen bonding in bent configurations due to a blue shift of this excitation.

1. Introduction

The stable tyrosyl radical is essential for the catalytic activity of class I ribonucleotide reductase (RNR). This enzyme catalyzes the reduction of ribonucleotides to deoxyribonucleotides, which are precursors in the synthesis of DNA.[1−4] It consists of two homodimeric proteins, R1 and R2. R1 contains the substrate binding site and R2 a diferric oxygen center and the neighboring tyrosyl radical. Tyrosyl radicals are found in RNR from different sources such as *Escherichia coli*, *Salmonella typhimurium*, mouse, and herpes simplex virus (HSV1), as well as in prostaglandin H synthase and photosystem II.[5−8] The tyrosyl residue that harbors the radical is embedded inside the protein at approximately 10 Å from the nearest protein surface and 5 Å from the diferric oxygen center in the crystal structure of the protein R2 moiety of *E. coli* RNR.[9] The distance between the radical and the substrate binding site is remarkably large, approximately 35 Å in the modeled complex between the two proteins R1 and R2.[10] A network of hydrogen-bonded amino acids connects the sites, and substitution of any of these amino acids inactivates the enzyme. Despite extensive research, the mechanisms for the enzymatic activity are not completely understood. The chemical communication between the radical and substrate was earlier suggested to be mediated by electron transfer (ET).[11] Previous findings, however, propose a coupled proton/electron transfer.[2,12] Theoretical studies by Siegbahn et al. indicate, in line with these findings, that ET is unlikely and propose a hydrogen atom transfer (HAT) to be the main mechanism.[13,14] By this mechanism, an entire hydrogen atom is transferred in each step of the passage through the hydrogen-bonded network. Using the spin-catalysis concept,[15] it has been suggested that the ground doublet state of the tyrosyl radical interacts with the triplet excited $\sigma\sigma^*$ state of the prolongated OH bond by intermolecular exchange (configuration interaction). The subsequent HAT along the hydrogen-bonded network was then interpreted as a triplet−triplet energy transfer through the protein chain.[16]

The tyrosyl radical has been studied by electron paramagnetic resonance (EPR) and electron−nuclear double resonance (ENDOR) spectra in many different RNRs.[5,6,8,17,18] A relatively large *g*-tensor anisotropy of the component directed along the CO bond of the tyrosyl ring, g_x, is detected by these EPR measurements. High-frequency EPR has been used for detailed studies of the *g*-anisotropy of the radical.[17−19] Such studies together with pulsed ENDOR experiments give evidence of lower g_x values in structures with protons near the tyrosyl radical.[17,18] These measurements have been carried out for tyrosyl radicals of RNR proteins from HSV1 and from mouse RNR where H-bonded deuterons were detected by ENDOR after deuterium exchange. The pulsed ENDOR spectrum was interpreted as due to a proton at a distance of 1.89 Å (mouse) and 1.96 Å (HSV1) from the phenolic oxygen.[17] On the basis of these findings, it has been suggested that the tyrosyl *g*-value is decreased by hydrogen bonding to the oxygen atom. Recent studies suggest that in certain systems there is a distribution of *g*-values that corresponds to a heterogeneous distribution of geometries for the hydrogen bond to the tyrosyl radicals.[20,21] Calculations of *g*-tensors may verify and explain these experimental results. Lately, semiempirical *g*-tensor calculations of the tyrosyl and phenoxyl radicals have been presented.[22,23] In this work, ab initio calculations of these types of radicals were

* Corresponding author. Fax: +46-13-137568; e-mail: maria@ifm.liu.se.
† Department of Physics, Stockholm University, Box 6730, SE-113 85 Stockholm, Sweden.
‡ Department of Biophysics, The Arrhenius Laboratories, SE-106 91 Stockholm, Sweden.
§ Theoretical Chemistry, Royal Institute of Technology SE-100 44 Stockholm, Sweden.
|| Center for Parallel Computers (PDC), Royal Institute of Technology SE-100 44 Stockholm, Sweden.

10.1021/jp0006633 CCC: $19.00
Published on Web 05/05/2000

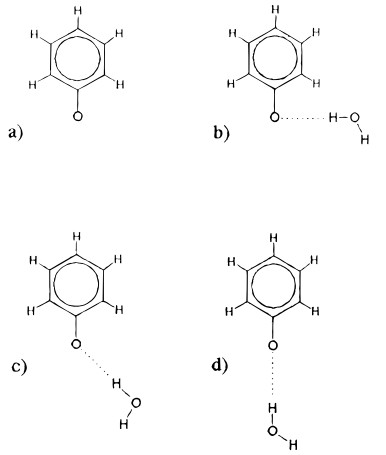

Figure 1. (a) Phenoxyl radical. (b) Phenoxyl radical with a water molecule as a model of a hydrogen bond at 90° with respect to the phenoxyl CO bond. (c) Phenoxyl radical with the water molecule in 135° orientation. (d) Phenoxyl radical and water molecule in linear configuration.

performed for the first time. The multiconfigurational self-consistent field (MCSCF) linear response method was used to calculate the *g*-shift as a sum of correction terms, that is, the dominating spin-orbit coupling (SOC) and orbital-Zeeman (OZ) cross-terms together with the relativistic mass and gauge corrections.[24,25] In addition, the excitation energies, SOC, and angular momentum (AM) matrix elements of the main interactions were calculated. By these calculations it was possible to trace the major electronic interactions contributing to the *g*-shift. According to the theory of Stone,[26,27] a lower *g*-value may be caused by reduction of the spin density on the oxygen atom[5] or an increased energy gap between the single occupied molecular orbital (SOMO) and oxygen lone-pair orbitals.[22] Calculations with the unrestricted Hartree−Fock (UHF)-MNDO (modified Neglect of Diatomic Overlap) method by Un et al. resulted in a lower *g*-value of a hydrogen-bonded methylphenoxy radical compared with the isolated radical.[22] The aim of this work is to test the hypothesis that hydrogen bonding of the tyrosyl radical induces a lower *g*-value from an ab initio approach and to give interpretations of the electronic mechanisms behind it. Detailed knowledge of spin excitation and redistribution upon H-bond formation, extracted from the *g*-tensor analysis, is essential for the spin chemistry because hydrogen bonding of the tyrosyl radical may be the first step of RNR catalytic activity.

2. Method

g-Values of the phenoxyl radical and phenoxyl−water complex (Figure 1) were calculated with the MCSCF linear response method implemented in a local version of the DALTON quantum chemistry program.[24,28] The *g*-values are calculated as a shift Δg from the free electron value, $g_e = 2.002319$. The *g*-shift is dominated by the SOC and OZ cross-terms in the one- and two-electron parts of the SOC operator [$\Delta g_{SOC/OZ}(1e)$, $\Delta g_{SOC/OZ}(2e)$]. Relativistic mass (Δg_{RMC}) and gauge corrections [$\Delta g_{GC}(1e)$, $\Delta g_{GC}(2e)$] provide minor contributions. Calculated *g*-shifts in this work were based on the following corrections[29]

$$\Delta g^{ab} = \Delta g_{RMC}\,\delta^{ab} + \Delta g_{GC}(1e) + \Delta g_{SOC/OZ}(1e) + \Delta g_{SOC/OZ}(2e) \quad (1)$$

The two-electron gauge correction was not included. This contribution is not expected to influence *g*-values significantly, except in those cases when the *g*-shift is close to zero. Earlier work by the present authors describe the different contributions of the *g*-shift in detail.[25,30]

TABLE 1: Phenoxyl *g*-Tensor with Different Complete Active Spaces (CAS)

CAS	g_x	g_y	g_z
3 × 3	2.0269	2.0063	2.0024
5 × 5	2.0110	2.0054	2.0024
7 × 7	2.0087	2.0050	2.0025
9 × 9	2.0086	2.0046	2.0025
11 × 11	2.0086	2.0046	2.0025

[a] $n \times n$ is an abbreviation for n electrons in n orbitals.

The B3LYP/6-31G** geometry optimizations were performed with the Gaussian98 program.[31] The phenoxyl radical was oriented in the *xy*-plane with the CO bond along the *x*-axis. MCSCF wave functions with correlating π orbital complete active space (CAS) and cc-pVDZ basis set were used in the calculations, that is, 7 electrons in 7 orbitals (7 × 7) of the isolated phenoxyl radical and 9 electrons in 9 orbitals (9 × 9) of the phenoxyl−water complex. The phenoxyl radical was assigned a $^2B_1$ ground state (the π-radical).

3. Results and Discussion

The spin density of the tyrosyl radical is localized to the oxygen atom and ring carbons in an alternating pattern.[32,33] Amino and carboxyl groups are not expected to contribute appreciably to the *g*-value as the unpaired electron resides entirely on the phenoxyl side chain.[22] Experimental EPR *g*-values of the tyrosyl and phenoxyl radicals are also very similar.[34,35] Accordingly, calculations of the phenoxyl radical are anticipated not to differ significantly from those of the tyrosyl radical. For these reasons, the phenoxyl radical was used as a model system. In the present study *g*-tensors were calculated with the ab initio linear response method.[24,25] Earlier studies show that restricted Hartree−Fock reference states yield satisfactory results for several substituted benzene radicals except for the phenoxyl radical.[30,36] This discrepancy is explained by a complex electronic structure with strong correlation, and to the presence of low-lying excited states. However, MCSCF wave functions with cc-pVDZ basis set yield *g*-values consistent with experiments.[30] MCSCF calculations of the SOC integrals are computationally demanding, and the cost increases rapidly with the increase of the number of atoms and the decrease of symmetry in the molecular system. Thus, in the present study, the CAS was optimized regarding highest accuracy at lowest computational effort. UHF natural orbital occupational numbers guided the choice of active space, and each occupied CAS orbital was assigned a correlated virtual orbital. The phenoxyl g_x value was strongly dependent on the active space (Table 1). Smaller active space than the full π-orbital (7 × 7) CAS yielded g_x values far too high, both regarding experimental values and CAS convergence. The results for the 9 × 9 and 11 × 11 CAS were identical at 4-decimal accuracy. On the basis of these calculations the 7 × 7 CAS was chosen as an appropriate active space. According to the literature, MCSCF wave functions with full π-orbital CAS and a basis set with polarization functions are necessary for an adequate description of the phenoxyl radical electronic structure.[37−39]

An experimental geometric structure is not available for the phenoxyl radical. Unfortunately, various problems connected with the determination of a proper CO bond length are reported in the literature.[36,37,39−42] Calculations based upon different methods (Restricted Open shell Hartree−Fock (ROHF), UHF, MCSCF, Density Functional Theory (DFT)) generate bond

TABLE 2: Experimental *g*-Tensor of Tyrosyl Radical in RNR from Different Sources Compared with Calculated Values for Phenoxyl + Water Complexes

	hydrogen bond	g_x	g_y	g_z
E. coli RNR[22]	−	2.0087	2.0042	2.0020
S. typhimurium RNR[5]	−	2.0089	2.0043	2.0021
Phenoxyl (this work)	−	2.0087	2.0050	2.0025
HSV1 RNR[17]	+	2.0076	2.0043	2.0022
mouse RNR[17]	+	2.0076	2.0043	2.0022
phenoxyl + water R(O···H) = 1.95	+	2.0081	2.0049	2.0025
phenoxyl + water R(O···H) = 1.70	+	2.0079	2.0048	2.0025
phenoxyl + water R(O···H) = 1.50	+	2.0076	2.0047	2.0025
phenoxyl + water 180° [a]	+	2.0081	2.0049	2.0025
phenoxyl + water 135° [a]	+	2.0078	2.0049	2.0025
phenoxyl + water 90° [a]	+	2.0074	2.0049	2.0025

[a] R(O···H) 1.95.

lengths in the range 1.22−1.38 Å. Predictions of the ground-state symmetry strongly depend on the starting guess for zero-iteration, and two main predictions for the ground state of the phenoxyl radical are reported. Some authors have assigned the phenoxyl radical a $^2B_2$ symmetry, which is the σ-radical with the unpaired electron on the *n*-orbital of the oxygen atom.[39,40] However, the most reliable MCSCF treatment with π-CAS (7 × 7) and large basis set by Chipman et al.[37] and also DFT calculations by Qin and Wheeler[33,42] predicted the ground-state π-radical ($^2B_1$). These authors also give a good agreement with experiments on hyperfine EPR structure and IR spectra. In this work, the $^2B_1$ ground state of the phenoxyl radical (the π-radical) was obtained by the ROHF method.

The *g*-tensor of the phenoxyl radical is sensitive to the geometric structure and it is therefore necessary to carry out a careful investigation of the *g*-tensor geometry dependence. In this work, a B3LYP-optimized CO distance of 1.26 Å was used as a starting point of the molecular structure studies. The hydrogen bond was simulated with a water molecule close to the phenoxyl oxygen. van Dam et al. propose that the hydrogen bond in mouse RNR is directed 20° out of the phenoxyl plane with the O···H bond in the plane normal to the ring and passing through the C_4-C_1-O axis.[17] The water molecule was oriented with the experimental structure as prototype. However, in-plane symmetry was used for technical reasons, reducing the computational effort and keeping the π-orbitals out of the phenoxyl plane. The geometrical influence on the *g*-tensor was investigated by simulations with changed phenoxyl CO bond length as well as variations in hydrogen bond distance and angle.

3.1. Phenoxyl Radical. The experimental *g*-tensor anisotropy was reflected in the calculated values (Table 2). The principal components of the *g*-tensor with the 7 × 7 CAS were g_x = 2.0087 directed along the CO bond, g_y = 2.0050 in the plane of the phenoxyl ring, and g_z = 2.0025 out of the phenoxyl plane. SOC and OZ cross-terms provided the major contribution to the in-plane components, $(SOC/OZ)_x$ = 6363 parts per million (ppm) and $(SOC/OZ)_y$ = 2600 ppm. These contributions consist of SOC integrals and AM matrix elements in the numerator and energy differences between ground and excited states in the denominator. The used MCSCF response method for *g*-tensor calculations includes thousands of contributions from all single excitations in the spectrum. However, the main contribution to g_x originated from the the lowest electronic transition $^2B_1 \rightarrow {}^2B_2$, which actually includes a single electron excitation from the oxygen lone-pair $n(b_2)$-orbital to the single occupied molecular orbital π-SOMO (b_1). The SOC integral, SOC = 35.38 cm^{-1}, and the AM matrix element, AM = 0.75, for this transition are both relatively large, whereas the excitation

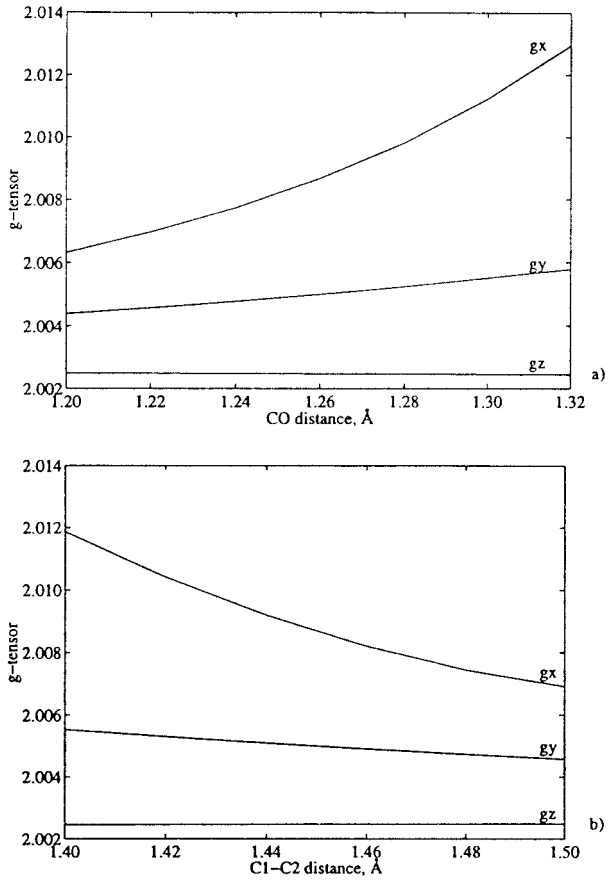

Figure 2. (a) Phenoxyl radical *g*-values as a function of CO distance. (b) Phenoxyl radical *g*-values as a function of C_1-C_2 distance.

energy is small, ΔE = 2.17 eV. The in-plane value g_y emanates mostly from the interaction between the π $^2B_1$ ground and σ $^2A_1$ excited states, with ΔE = 6.66 eV, SOC = 29.97 cm^{-1}, and AM = 0.92. The rather high excitation energy was compensated for by large values of the SOC integrals and AM matrix elements. Gauge and relativistic mass corrections were one order of magnitude smaller than the in-plane SOC/OZ terms. A low-lying $^2A_2$ excited state with excitation energy 2.56 eV contributes to the out-of-plane component g_z. Despite this small energy gap, the *g*-shift Δg_z was close to zero, which could be explained by a weak spin-orbit interaction between π-states, SOC = 0.01 cm^{-1}. The SOC/OZ contribution was small, $(SOC/OZ)_z$ = 147 ppm, and the relativistic mass correction was negative, $(RMC)_z$ = −197 ppm.

Semiempirical UHF-MNDO calculations by Un et al. did not yield significantly different *g*-values upon changes in the CO bond distance from 1.24 Å to 1.26 Å.[22] Furthermore, *g*-values by this method are insensitive to small variations of the phenoxyl ring geometry. In contrast to these results, calculations in this work showed significant changes in the *g*-values as a function of CO bond length: g_x at CO distance 1.24 Å was 2.0078, whereas g_x = 2.0087 at CO distance 1.26 Å (Figure 2a). This performance could be explained by a decreased $n \rightarrow \pi_{SOMO}$ excitation energy together with increased SOC and AM matrix elements at increased CO bond lengths (Figure 3). Experimental observations and calculations of energies and vibrational frequencies by Ivancich et al. indicate that the CO bond distance decreases at decreased hydrogen bond distance until hydrogen bond equilibrium is reached.[20] Thus, hydrogen bonding may influence the CO bond length. Variation of C_1-C_2 bond lengths also resulted in substantial differences: g_x = 2.0093 at R(C_1-C_2) = 1.44 Å, whereas g_x = 2.0083 at R(C_1-C_2) = 1.46 Å

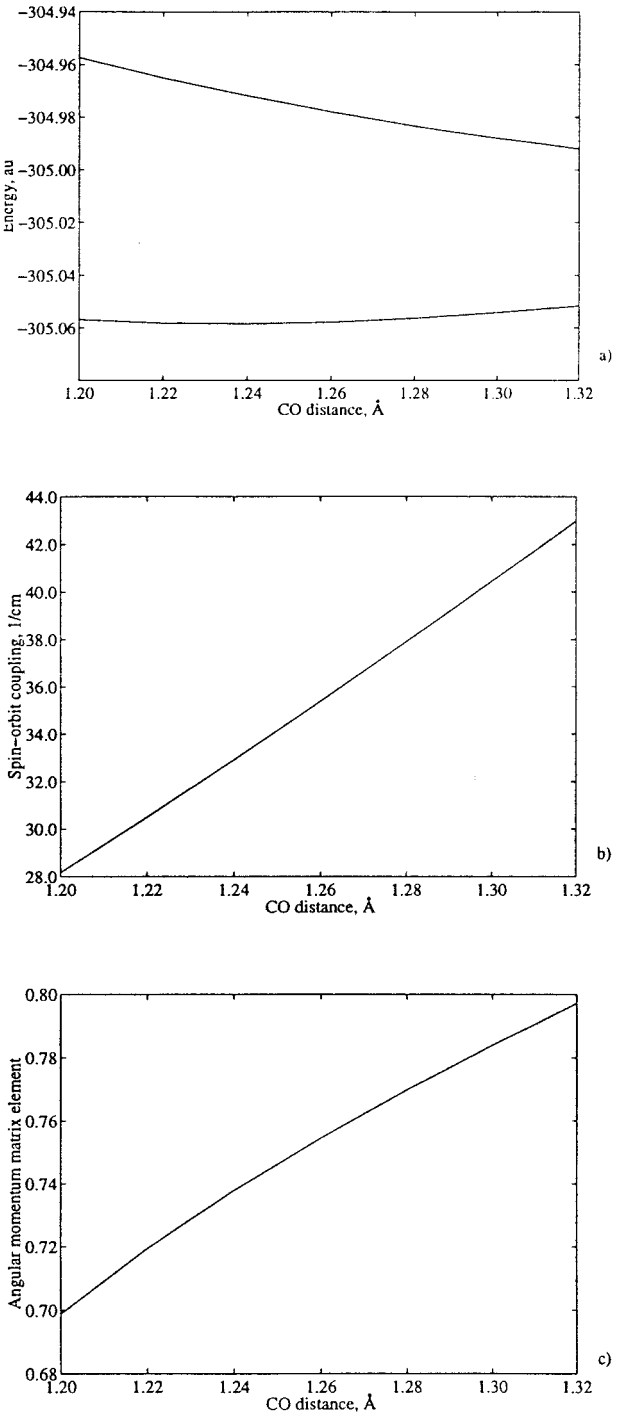

Figure 3. Energies of the $^2B_1$ and $^2B_2$ states (a), SOC (b), and AM matrix elements (c) for these states (the $n \rightarrow \pi_{SOMO}$ excitation), which provide the major contribution to the g_x value of the phenoxyl radical.

(Figure 2b). These calculations were performed by narrowing and extending the phenoxyl ring in the *y*-direction.

Calculated *g*-values were sensitive to the choice of active space. This sensitivity could be traced to strong correlation and strong coupling between the low-lying excited states. Excitation energies of the two lowest excited states B_2 and A_2 were 2.17 eV and 2.56 eV, respectively, at the B3LYP equilibrium ground-state geometry. A potential energy surface crossing for these two states near the MCSCF ground-state minimum at CO distance 1.23 Å was observed (Figure 4). The 7 × 7 CAS yielded results in agreement with experiment, whereas smaller CAS resulted in overestimated *g*-values. Interestingly, inclusion

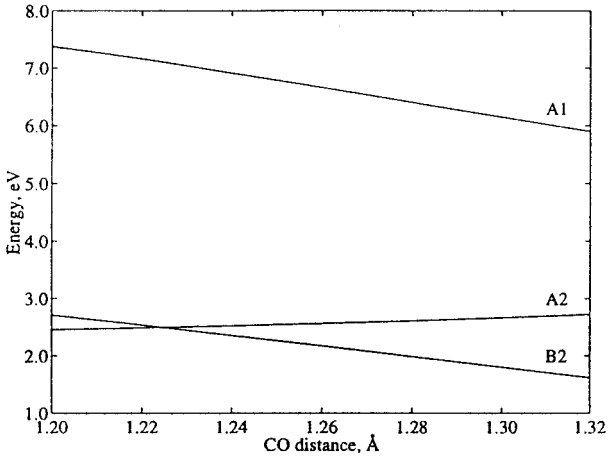

Figure 4. Excitation energies from the ground to the lowest states of $^2A_1$, $^2A_2$, and $^2B_2$ symmetry. These states contribute to the g_y, g_z, and g_x components, respectively.

TABLE 3: Excitation Energies, SOC, and AM Matrix Elements of the $^2B_1 \rightarrow {}^2B_2$ ($n \rightarrow \pi_{SOMO}$ Excitation

	energy (eV)	SOC (cm^{-1})	AM
phenoxyl	2.17	35.38	0.75
phenoxyl + water R(O···H) = 1.95	2.12	33.63	0.69
phenoxyl + water R(O···H) = 1.70	2.13	32.91	0.69
phenoxyl + water 180° [a]	2.12	33.63	0.69
phenoxyl + water 135° [a]	2.23	33.58	0.70
phenoxyl + water 90° [a]	2.46	33.85	0.70

[a] R(O···H) = 1.95.

of the oxygen lone pair (b_2 orbital) to the active space did not affect the result appreciably.

3.2. Hydrogen Bonding. 3.2.1. Linear Model. As a first step the hydrogen bonding was simulated with one water molecule in a linear configuration with respect to the phenoxyl CO bond (Figure 1d). This configuration is the simplest model of H-bonding in the phenoxyl−water complex; it does not correspond to the real equilibrium structure, which is actually bent. B3LYP/6-31G** geometry optimizations of the phenoxyl−water complex yielded the following structural parameters: ∠C−O−H = 112.5°, R(O···H) = 1.94 Å, R(C−O) = 1.26 Å, ∠O−H−O = 160.6°.

Inclusion of a water molecule at the hydrogen bonding distance R(O···H) = 1.95 Å lowered the g_x value from 2.0087 to 2.0081 (Table 2). The *g*-tensor showed only a slight dependence on the hydrogen bond distance: g_x = 2.0079 at R(O···H) = 1.70 Å and g_x = 2.0076 at R(O···H) = 1.50 Å. Examination of the individual components contributing to the SOC/OZ term showed that the excitation energy of the most important $n \rightarrow \pi_{SOMO}$ excitation was lowered in the linear phenoxyl−water complex compared with the isolated phenoxyl radical (Table 3). This could imply a higher g_x value upon hydrogen bonding but, in contrast, the g_x value was decreased. The lower excitation energy in the denominator is thus compensated for by the terms in the numerator. That is, the lower g_x value in the phenoxyl−water linear model depends on the lower SOC and AM matrix elements (Tables 2 and 3). The *g*-value was also reduced upon a decreased hydrogen bond distance. This reduction could be traced to a lower SOC constant for R(O···H) = 1.70 Å compared with R(O···H) = 1.95 Å.

3.2.2. Bent Models. The B3LYP geometry optimizations of the phenoxyl−water complex gave a nonlinear C═O···H bond with the angle ∠C−O−H = 112.5° with an almost plane "phenoxyl ring + C═O···H−O" structure (the dihedral angle

was 20.9°). The bond length O···H was obtained equal to 1.94 Å. The *g*-values for the phenoxyl−water model in the more realistic bent configurations were calculated for a few nonlinear structures (Figure 1b−c). The hydrogen bonding distance was kept at R(O···H) = 1.95 Å and the angles ∠C−O−H were fixed equal to 135° and 90° to simulate different extreme structures. The g_x component was decreased as the position of the water molecule changed from a linear to a right-angled configuration. That is, $g_x(180°) = 2.0081$, $g_x(135°) = 2.0078$, and $g_x(90°) = 2.0074$. In this case, the decrease in g_x value is traced to an increase in the excitation energy of the $n \rightarrow \pi_{SOMO}$ transition: $\Delta E(180°) = 2.12$ eV, $\Delta E(135°) = 2.23$ eV, and $\Delta E(90°) = 2.46$ eV. The different performance between the linear and bent models can be explained by the shape of the oxygen lone-pair orbital. The oxygen lone-pair *n* is the p_y orbital, and a phenoxyl−water complex in bent configuration produces an overlap between the phenoxyl *n* and water molecular orbitals that is not produced in the linear configurations.

The AM matrix elements remained basically unaltered for all hydrogen-bonding models. The SOC integral, however, shows small variations depending on both hydrogen bond length and angle.

4. Conclusions

The calculated *g*-tensors according to the phenoxyl and phenoxyl−water models were comparable with experimental observations of the tyrosyl radical. That is, the calculations reproduced the anisotropy of the tyrosyl radical as well as the shift of g_x toward lower values upon hydrogen bonding that was observed experimentally for mouse and HSV1 RNR.[17] The other two components, g_y and g_z, were not affected by the presence of a hydrogen bond.

Interestingly, the $n \rightarrow \pi$ ($^2B_1 \rightarrow {}^2B_2$) excitation was scarcely affected by hydrogen bonding in the linear configurations. However, the strong blue shift of this transition upon bent H-bond formation is the most prominent feature of the tyrosyl−water interaction. Together with the small reduction of the $\langle L_x \rangle$ integral and the SOC matrix element it explained the characteristic lowering of the g_x term. The blue shift of the $n \rightarrow \pi$ transitions in polar solvents is well known for a number of stable diamagnetic molecules with the singlet ground state when a hydrogen bond is formed to the atom on which the nonbonding orbital (lone pair *n*) is located.[43] Here we predict that a similar blue shift is typical for the $n \rightarrow \pi_{SOMO}$ transition in a π-radical like phenoxyl upon H-bond formation.

Acknowledgment. This work was supported by the Swedish Foundation for Strategic Research via the graduate school Forum Scientum and the Swedish Natural Science Research Council (AG). Computer time has been supported by PDC, Center for Parallel Computers, at KTH, Stockholm.

References and Notes

(1) Fontecave, M.; Pierre, J.-L. *Bull. Soc. Chim. Fr.* **1996**, *133*, 653.
(2) Gräslund, A.; Sahlin, M. *Annu. Rev. Biophys. Biomol. Struct.* **1996**, *25*, 259.
(3) Reichard, P. *Science* **1993**, *260*, 1773.
(4) Stubbe, J.; van der Donk, W. A. *Chem. Biol.* **1995**, *2*, 793.
(5) Allard, P.; Barra, A. L.; Andersson, K. K.; Schmidt, P. P.; Atta, M.; Gräslund, A. *J. Am. Chem. Soc.* **1996**, *118*, 895.
(6) Barry, B. A.; Babcock, G. T. *Proc. Natl. Acad. Sci. U.S.A.* **1987**, *84*, 7099.
(7) Kauppi, B.; Nielsen, B. B.; Ramaswamy, S.; Larsen, I. K.; Thelander, M.; Thelander, L.; Eklund, H. *J. Mol. Biol.* **1996**, *262*, 706.
(8) Ma, C.; Barry, B. A. *Biophys. J.* **1996**, *71*, 1961.
(9) Nordlund, P.; Sjöberg, B.-M.; Eklund, H. *Nature* **1990**, *245*, 593.
(10) Uhlin, U.; Eklund, H. *Nature* **1994**, *370*, 533.
(11) Voet, D.; Voet, J. G. *Biochemistry*; J. Wiley: New York, 1995.
(12) Ekberg, M.; Sahlin, M.; Eriksson, M.; Sjöberg, B.-M. *J. Biol. Chem.* **1996**, *271*, 20655.
(13) Siegbahn, P. E. M.; Blomberg, M.; Pavlov, M. *Chem. Phys. Lett.* **1998**, *292*, 421.
(14) Siegbahn, P. E. M.; Eriksson, L.; Himo, F.; Pavlov, M. *J. Phys. Chem.* **1998**, *102*, 10622.
(15) Minaev, B. F. *Theor. Exp. Chem.* **1996**, *32*, 1.
(16) Minaev, B. F.; Ågren, H., to be submitted for publication.
(17) van Dam, P. J.; Willems, J.-P.; Schmidt; P. P.; Pötsch, S.; Barra, A.-L.; Hagen, W. R.; Hoffman, B. M.; Andersson, K. K.; Gräslund, A. *J. Am. Chem. Soc.* **1998**, *120*, 5080.
(18) Schmidt, P. P.; Andersson, K. K.; Barra, A.-L.; Thelander, L.; Gräslund, A. *J. Biol. Chem.* **1996**, *271*, 23615.
(19) Gerfen, G. J.; Bellew, B. F.; Un, S.; Bollinger, J. M. J.; Stubbe, J.; Griffin, R. G.; Singel, D. J. *J. Am. Cihem. Soc.* **1993**, *115*, 6420.
(20) Ivancich, A.; Mattioli, T. A.; Un, S. *J. Am. Chem. Soc.* **1999**, *121*, 5743.
(21) Liu, A.; Barra, A.-L.; Rubin, H.; Lu, G.; Gräslund, A. *J. Am. Chem. Soc.* **2000**, *122*, 1974.
(22) Un, S.; Atta, M.; Fontecave, M.; Rutherford, A. W. *J. Am. Chem. Soc.* **1995**, *117*, 10713.
(23) Gerfen, G. J.; Bellew, B. F.; Griffin, R. G.; Singel, D. J.; Ekberg, C. A.; Whittaker, J. W. *J. Phys. Chem.* **1996**, *100*, 16739.
(24) Vahtras, O.; Minaev, B.; Ågren, H. *Chem. Phys. Lett.* **1997**, *281*, 186.
(25) Engström, M.; Minaev, B.; Vahtras, O.; Ågren, H. *Chem. Phys.* **1998**, *237*, 149.
(26) Stone, A. J. *Mol. Phys.* **1963**, *6*, 509.
(27) Stone, A. J. *Mol. Phys.* **1964**, *7*, 311.
(28) Helgaker, T.; Jensen, H. J. A.; Jørgensen, P.; Olsen, J.; Ruud, K.; Ågren, H.; Andersen, T.; Bak, K. L.; Bakken, V.; Christiansen, O.; Dahle, P.; Dalskov, E. K.; Enevoldsen, T.; Fernandez, B.; Heiberg, H.; Hettema, H.; Jonsson, D.; Kirpekar, S.; Kobayashi, R.; Koch, H.; Mikkelsen, K. V.; Norman, P.; Packer, M. J.; Saue, T.; Taylor, P. R.; Vahtras, O. DALTON, a second-order MCSCF molecular property program.
(29) Harriman, J. E. *Theoretical Foundations of Electron Spin Resonance*; Academic Press: New York, 1978.
(30) Engström, M.; Vahtras, O.; Ågren, H. *Chem. Phys.* **1999**, *243*, 263.
(31) Frisch, M. J.; Trucks, G. W.; Schlegel, H. B.; Scuseria, G. E.; Robb, M. A.; Cheeseman; J. R.; Zakrzewski, V. G.; Montgomery, J. A. J.; Stratmann, R. E.; Burant, J. C.; Dapprich, S.; Millam, J. M.; Daniels, A. D.; Kudin, K. N.; Strain, M. C.; Farkas, O.; Tomasi, J.; Barone, V.; Cossi, M.; Cammi, R.; Mennucci, B.; Pomelli, C.; Adamo, C.; Clifford, S.; Ochterski, J.; Petersson, G. A.; Ayala, P. Y.; Cui, Q.; Morokuma, K.; Malick, D. K.; Rabuck, A. D.; Raghavachari, K.; Foresman, J. B.; Cioslowski, J.; Ortiz, J. V.; Stefanov, B. B.; Liu, G.; Liashenko, A.; Piskorz, P.; Komaromi, I.; Gomperts, R.; Martin, R. L.; Fox, D. J.; Keith, T.; Al-Laham, M. A.; Peng, C. Y.; Nanayakkara, A.; Gonzalez, C.; Challacombe, M.; Gill, P. M. W.; Johnson, B.; Chen, W.; Wong, M. W.; Andres, J. L.; Gonzalez, C.; Head-Gordon, M.; Replogle, E. S.; Pople, J. A. Gaussian 98, Revision A.5; Gaussian, Inc., Pittsburgh, PA, 1998.
(32) Himo, F.; Gräslund, A.; Eriksson, L. A. *Biophys. J.* **1997**, *72*, 1556.
(33) Qin, Y.; Wheeler, R. A. *J. Am. Chem. Soc.* **1995**, *117*, 6083.
(34) Bresgunov, A. Y.; Dubinsky, A. A.; Poluektov, O. G.; Lebedev, Y. S. *Mol. Phys.* **1992**, *75*, 1123.
(35) Fasanella, E. L.; Gordy, W. *Proc. Natl. Acad. Sci. U.S.A.* **1969**, *62*, 299.
(36) Mestechkin, M. M.; Poltavets, V. N.; Degtyarev, L. S.; Pohodenko, V. D. *Theor. Exp. Chem.* **1984**, *20*, 78.
(37) Chipman, D. M.; Liu, R.; Zhou, X.; Pulay, P. *J. Chem. Phys.* **1994**, *100*, 5023.
(38) Bofill, J. M.; Pulay, P. *J. Chem. Phys.* **1989**, *90*, 3637.
(39) Yu, H.; Goddard, J. D. *J. Mol. Struct.: THEOCHEM* **1991**, *233*, 129.
(40) Luzhkov, V. B.; Zyubin, A. S. *J. Mol. Struct. THEOCHEM* **1988**, *170*, 33.
(41) Nwobi, O.; Higgins, J.; Zhou, X.; Liu, R. *Chem. Phys. Lett.* **1997**, *272*, 155.
(42) Qin, Y.; Wheeler, R. A. *J. Chem. Phys.* **1995**, *102*, 1689.
(43) Strickler, S. J.; Kasha. M. *J. Am. Chem. Soc.* **1963**, *85*, 2899.